Appl. Phys. A (2017) 123:231
DOI 10.1007/s00339-017-0837-1

Applied Physics A
Materials Science & Processing

TiO_2/WO_3 photoactive bilayers in the UV–Vis light region

E. Vasilaki[1,2] · D. Vernardou[2] · G. Kenanakis[2,3] · M. Vamvakaki[3,4] · N. Katsarakis[2,3]

Received: 8 November 2016 / Accepted: 6 February 2017 / Published online: 9 March 2017

Abstract In this work, photoactive bilayered films consisting of anatase TiO_2 and monoclinic WO_3 were synthesized by a sol–gel route. Titanium isopropoxide and tungsten hexachloride were used as metal precursors and deposition was achieved by spin-coating on Corning glass substrates. The samples were characterized by X-ray diffraction, photoluminescence, UV–Vis, and Raman spectroscopy, as well as field emission scanning electron microscopy. The prepared immobilized catalysts were tested for their photocatalytic performance by the decolorization of methylene blue in aqueous matrices, under UV–Vis light irradiation. The annealing process influenced the crystallinity of the bilayered films, while the concentration of the tungsten precursor solution and the position of the tungsten trioxide layer further affected their photocatalytic performance. In particular, the photocatalytic performance of the bilayered films was optimized at a concentration of 0.1 M of the WO_3 precursor solution, when deposited as an overlying layer on TiO_2 by two annealing steps (~76% methylene blue decolorization in 300 min of irradiation versus ~59% in the case of a bare TiO_2 film). In general, the coupled layer catalysts exhibited superior photoactivity compared to that of bare TiO_2 films with WO_3 acting as an electron trap, resulting, therefore, in a more efficient electron–hole separation and inhibiting their recombination.

✉ E. Vasilaki
euavasilakh@gmail.com

[1] Department of Chemistry, University of Crete, 71003 Heraklion, Crete, Greece

[2] Center of Materials Technology and Photonics, School of Engineering, Technological Educational Institute of Crete, 71004 Heraklion, Crete, Greece

[3] Institute of Electronic Structure and Laser, Foundation for Research and Technology-Hellas, Vassilika Vouton, P.O. Box 1385, 711 10 Heraklion, Crete, Greece

[4] Department of Materials Science and Technology, University of Crete, 71003 Heraklion, Crete, Greece

1 Introduction

Heterogeneous photocatalysis is one of the most promising advanced oxidation processes (AOPs) targeting the efficient mineralization of inorganic and organic pollutants. TiO_2 has been the catalyst of choice for a wide range of photocatalytic applications. However, the maximization of its efficiency is inhibited by its bandgap (~3.0–3.2 eV) that limits the exploitation of solar energy and its high recombination rate of photoinduced charge carriers [1]. Numerous efforts have been conducted for the improvement of its performance, while amongst them, coupling with other semiconductors has been the subject of intensive research. In this context, modification of TiO_2 with WO_3 leads to higher photoactivity than that of bare TiO_2 [2, 3]. This occurs, because its small bandgap (~2.5–2.8 eV) provides strong absorption within the solar spectrum, while photochemical stability and resilience to photocorrosion are among its main merits [4].

Up so far, the majority of research regards coupled TiO_2/WO_3 photocatalysts in powder form [5–9]. However, the need for reuse and environmental safety demands for immobilized catalysts. Towards this direction, TiO_2/WO_3 semiconductors have been prepared by mixing their precursor solutions at different ratios. Pan et al. [10] prepared mesoporous WO_3/TiO_2 thin films by one mixed precursor solution and evaluated their photocatalytic activity in decomposing 2-propanol in the gas phase under UV–Vis light irradiation. Their performance was optimized at 4 mol% of WO_3 concentration, being 2.2 and 6.1 times

higher than that of a bare mesoporous TiO_2 film and a nonporous TiO_2 film, respectively. This enhancement was ascribed to an increase in surface acidity. Fu et al. [11] fabricated TiO_2/WO_3 hybrid films on quartz substrates by a simple dip coating method followed by a heating post-treatment using a mixed precursor sol and tested their photoactivity under visible light with respect to degradation of 4-chlorophenol. In this case, the TiO_2/WO_3 hybrid film exhibited a higher degradation and mineralization efficiency than pure TiO_2 film.

Patrocinio et al. [12] deposited 30 alternating layers of TiO_2 and WO_3 sols onto fluorine doped tin oxide (FTO) substrates employing a layer-by-layer technique. The hybrid films exhibited higher photonic efficiencies and degradation rates of acetaldehyde than those of pure self-assembled TiO_2 films under UV-A irradiation. Furthermore, Bojinova et al. [13] tested the efficiency of WO_3/TiO_2 films in degrading malachite green in water solutions, under UV and visible-light irradiation, and concluded that the films with 10% of WO_3 exhibited better photocatalytic activity than the pure TiO_2 films. Oliveira et al. [2] deposited bilayered porous films of TiO_2 with underlying WO_3 on transparent electrodes, exhibiting improved efficiency for Rhodamine 6G photodegradation under polychromatic irradiation, due to the enhanced light harvesting and reduced charge recombination. On the other hand, Miyauchi et al. [14] prepared anatase TiO_2 films on which layers of amorphous (a-WO_3) or triclinic WO_3 (c-WO_3) were deposited. In this case, evaluation of the photocatalytic activity of the heterogeneous films by decomposition of adsorbed methylene blue under UV illumination showed that a-WO_3 and c-WO_3 did not enhance the photocatalytic oxidation activity of TiO_2.

Among the deposition methods, the chemical routes using solutions have advantages such as simplicity, low cost, and environmentally friendly precursors. In addition, the characteristics of the bilayers can simply be controlled via the alteration of the solution concentration, temperature, and time [15]. As observed above, the modification of TiO_2 with WO_3 in a film form by a single mixed precursor sol has thoroughly been investigated. On the other hand, it has been reported that in the case of mixed oxides, the crystallization of the composite film can be significantly hindered, an impediment that can be overcome in bilayered films [10, 16]. However, there is not a systematic study regarding bilayered films of TiO_2/WO_3 that evaluates the effect of important parameters, such as the position of the tungsten oxide layer and the concentration of the precursor solutions on their photocatalytic activity. Hence, this study aims to systematically investigate the photoactivity of TiO_2/WO_3 bilayered films on glass substrates towards the decolorization of an aqueous solution of methylene blue under UV–Vis light irradiation. Methylene blue was chosen as the target pollutant due to the alarming pollution levels caused to the aquatic life by colored waste waters, which are released in the ecosystem from textile industry and account for 15% of the total world production of dyes [17]. The effects of the annealing process, the concentration of the WO_3 precursor solution, and the tungsten trioxide layer's position on the TiO_2/WO_3 photocatalytic activity are considered.

2 Experimental details

2.1 Reagents

Titanium isopropoxide ($Ti[OCH(CH_3)_2]_4$) of 99.99% purity, tungsten (VI) chloride (WCl_6, >99.9%), methylene blue (MB), and hydrochloric acid (HCl, >37%) were supplied by Sigma-Aldrich and were used without further purification. Absolute ethanol was supplied by Fischer Scientific and Milli-Q Direct water was obtained from a Millipore apparatus with a resistivity of 18.2 MΩ at 298 K. Experiments were carried out at the natural pH corresponding to aqueous solutions of MB, i.e., pH at ca. 5.

2.2 Synthesis of the precursor solutions

The bilayered TiO_2/WO_3 films were prepared by a sol–gel method, using ethanolic solutions of $Ti[OCH(CH_3)_2]_4$ and WCl_6 for the titania and tungsten precursors, respectively. In the case of the TiO_2 precursor, a synthetic procedure reported elsewhere was followed [18, 19]. In particular, titanium isopropoxide (2.8 ml) was added to absolute EtOH (25 ml) and the solution was stirred for 15 min at 60 °C. A small volume of HCl was added dropwise to get an acidic solution and avoid precipitation, and the precursor was further stirred for 20 min at 60 °C [20]. The mechanism can be explained as follows: the titanium alkoxide is protonated in a rapid first step. This makes the Ti atom more electrophilic and susceptible to water. Following the deposition of the precursor solution on glass substrate, a transparent film is produced due to the evaporation of the solvent and hydrolysis of $Ti[OCH(CH_3)_2]_4$. Aggregation, gelation, and drying occur in seconds to minutes rather than days as in bulk sol–gel systems, and annealing of the film removes the alkoxy and hydroxyl groups, forming a Ti/O/Ti network.

For the tungsten precursor, an appropriate amount of WCl_6 was dissolved in absolute EtOH and a reaction of solvolysis took place. Gradual change of colour occurred: first, the solution turned yellow, and since ethanol was in excess, the replacement of chlorine ions by the ethoxide groups was completed in minutes. After a few minutes of stirring, $W(OC_2H_5)_6$ was formed, and the solution became

colourless. Finally, the solution turned to dark blue, indicating the formation of amorphous $WO_3 \cdot nH_2O$ [21, 22].

The deposition of the oxide layers was performed by spin-coating at 2000 rpm for 30 s on 10×10 mm^2 Corning Eagle 2000 Borosilicate Glass (Specialty Glass Products) substrates. Before deposition, the Corning glass substrates were cleaned using a piranha solution ($H_2SO_4/H_2O_2 = 3/1$), rinsed with ultrapure water, and dried under N_2 gas flow. For the needs of this work, four layers of TiO_2 were grown on the substrates and were overlaid by a single layer of WO_3, synthesized from precursor solutions of different concentrations (denoted as TiO_2/WO_3 films). After the deposition of each layer, the films were heated at 350 °C for 10 min to evaporate the solvent and remove the organic residuals. Then, crystallization was carried out by annealing at 500 °C for 2 h by two different routes: either once for the final bilayered TiO_2/WO_3 films (one annealing step), or twice (two annealing steps) after the alternation between the titanium and tungsten oxide layers. Finally, to evaluate the influence of the position of the tungsten trioxide layer, TiO_2 films underlaid by WO_3 were synthesized (denoted as WO_3/TiO_2 films) and their photocatalytic performance was compared to the aforementioned TiO_2 films with an overlying WO_3 layer.

2.3 Characterization and photocatalytic experiments

The samples were characterized by Raman spectroscopy at room temperature, on a Nicolet Almega XR Raman spectrometer (Thermo Scientific), with a 473 nm blue laser as an excitation source in the range of 50–1000 cm^{-1}. X-ray diffraction (XRD) patterns were collected on a Rigaku (RINT 2000) diffractometer with Cu *Ka* X-rays, while UV–Vis transmittance measurements were performed using a Perkin-Elmer Lambda 950 spectrometer over the wavelength range of 200–800 nm. The photoluminescence measurements were carried out using a He–Cd CW laser at 325 nm as the excitation source at room temperature. The spectra were recorded using a LN2 cooled CCD camera and a spectrometer with a UV blazed grating. The morphology of the surfaces was examined by field emission scanning electron microscopy (FE-SEM JEOLJSM-7000F).

For the photocatalytic evaluation, an aqueous solution of 15 mg/L of MB was used as the target pollutant. For the conduction of the photocatalytic experiments, the bilayered films of rectangular geometry (area of 10×10 mm^2) were placed at the bottom of a quartz cell and were covered by 1 ml of MB solution. The top of the cell was topped with a polycarbonate filter that cuts out the UV emission lines under 385 nm, as shown in Fig. 1a. The irradiation was carried out in a homemade reactor with aluminium reflector sides, while as irradiation source, five black light lamps (4 W, Philips TL 4W/08) that predominantly emit

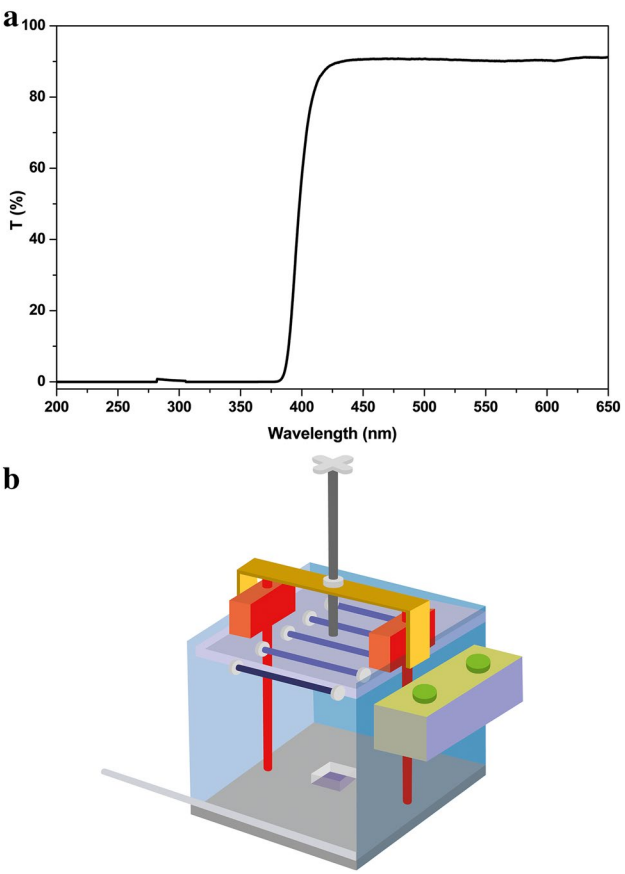

Fig. 1 **a** Transmittance spectrum of the polycarbonate filter and **b** the set up of the photoreactor used in this work

at 365 nm were used. The distance between cell and lamps was 13 cm, while the light intensity inside the reactor was ~1.6 mW/cm^2 [23]. The photocatalytic setup is illustrated in Fig. 1b. The rate of removal of MB was monitored by UV–Vis Spectroscopy using a Shimadzu UV-2401 spectrophotometer. Methylene blue presents a characteristic absorbance peak at 665 nm and to estimate the rate of decolorization, aliquots of the sample were withdrawn periodically for the record of their absorbance and were returned into the reactor immediately thereafter. Quantification of the removal was estimated by calculation of the area below the main MB peak in the range of 540–700 nm. Additional blank experiments without a catalyst were also performed as well as dye adsorption experiments in the dark.

3 Results and discussion

Figure 2 presents the Raman spectra of pure TiO_2 films and TiO_2/WO_3 (0.1 M) bilayers for one and two annealing steps, with WO_3 as an overlying layer. As can be seen in

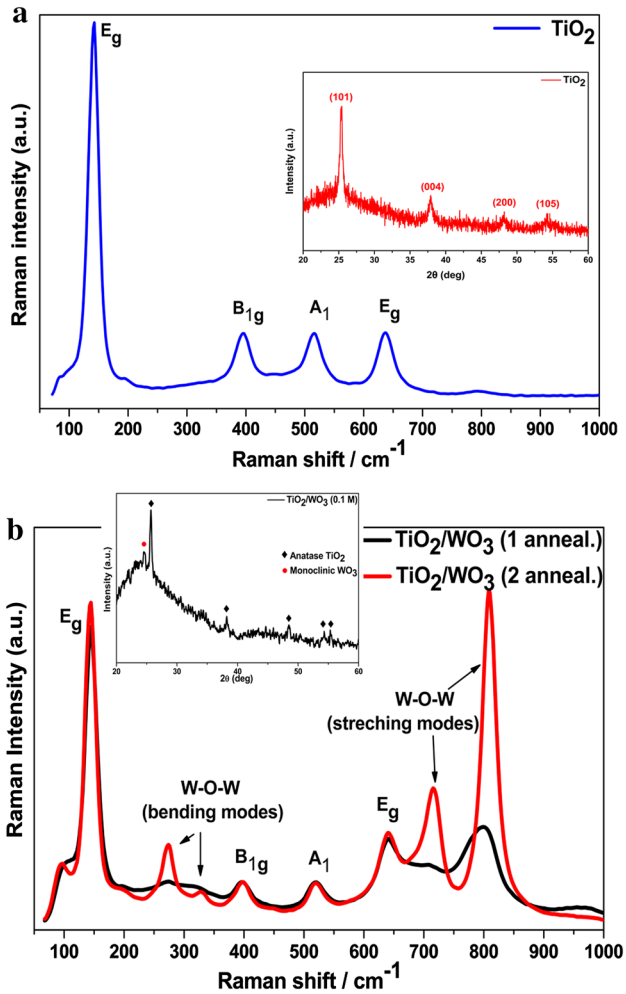

Fig. 2 Raman spectra of **a** bare TiO_2 film and **b** TiO_2/WO_3 (0.1 M) bilayers for one and two annealing steps. In the insets, the XRD patterns of the aforementioned immobilized catalysts are shown

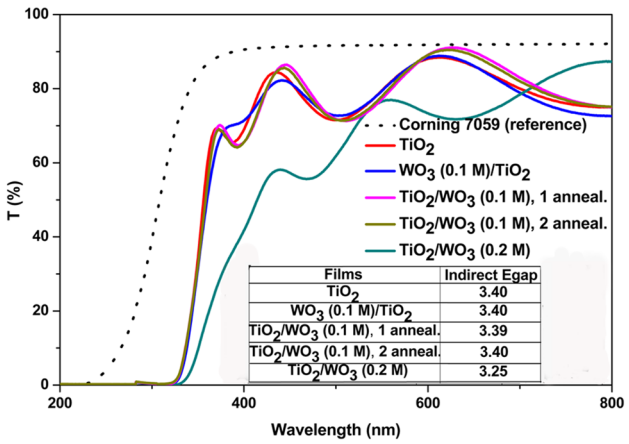

Fig. 3 Optical transmittance spectra of bare TiO_2 and bilayered TiO_2/WO_3 and WO_3/TiO_2 films. In the inset, the indirect optical energy band-gap values (E_{gap}, eV), as determined using "Tauc" plots of $(ah\nu)^n$ vs. photon energy for the estimation of indirect ($n=0.5$) optical band-gap energies

Fig. 2a, TiO_2 was formed at its anatase phase, with phonon frequencies matching within ±2 cm^{-1} with the literature: 144 cm^{-1} (E_g), 395 cm^{-1} (B_{1g}), 516 cm^{-1} (A_{1g}), and 637 cm^{-1} (E_g) [24]. The inset of Fig. 2a shows the XRD pattern of a bare TiO_2 film, displaying diffraction peaks at 2θ values of 25.4°, 37.9°, 48.2°, and 54.3° with Miller indices (101), (004), (200), and (105) respectively, which further confirms the formation of the TiO_2 anatase phase. Furthermore, in the case of two annealing steps, as presented in Fig. 2b, apart from the anatase phase of TiO_2, the monoclinic WO_3 phase was also present at 273 and 329 cm^{-1} due to the W–O–W bending modes of bridging oxide ions, as well as at 718 and 810 cm^{-1} corresponding to the W–O–W stretching mode (tungsten oxide network) [21, 25]. A significant increase in the signal-to-noise ratio is shown for the two compared with the one annealing step, with the Raman peaks becoming at the same time more intense and narrow. In the inset of Fig. 2b, the XRD pattern of the TiO_2 film with an overlying layer of WO_3 (0.1 M) synthesized by two annealing steps is presented. It exhibits five characteristic diffraction peaks at 2θ of 25.7°, 38.2°, 48.5°, 54.3°, and 55.3° with Miller indices (101), (004), (200), (105), and (211) respectively, which were all attributed to the anatase TiO_2 phase, as well as a low intensity peak at 24.4°, i.e., with (002) Miller indices, due to monoclinic WO_3 [13, 26]. There was no discrepancy observed among the X-ray diffraction patterns for one and two annealing steps (one annealing step pattern is not shown here for brevity). Although XRD gave no indication of the majority of monoclinic WO_3 peaks, as the crystallization temperature of WO_3 is relatively higher than that of TiO_2 [27], Raman analysis proved the presence of both anatase TiO_2 and monoclinic WO_3 depending on the annealing procedure followed, as the two annealing steps process enhanced the presence of well-formed anatase TiO_2 and monoclinic WO_3. This happens, because XRD is known to probe the long-range order crystallinity of materials, while Raman is a probe of the influence of even localized short-range order to the vibrational modes of bond configurations [27, 28]. Hence, one may say that the TiO_2/WO_3 films (independently of the annealing procedure followed) are of low crystallinity, maintaining, however, a short-range crystalline ordering as also explained in the previous works [29, 30].

The optical transmittance spectra of the synthesized thin films in the wavelength range of 200–800 nm are presented in Fig. 3. All thin films are highly transparent in the visible wavelength region with an average transmittance of about 70–90%, with a fall-off for wavelengths shorter than 350 nm. Furthermore, the indirect optical energy gap values (E_{gap}) of the films were determined by

the extrapolation of the linear portion of $(ahv)^n$ vs. hv plots ("Tauc" plots), where $n = 0.5$. The band-gap value obtained for the bare TiO_2 thin films is 3.40 eV, in good accordance to the one reported for anatase TiO_2 thin films obtained by sol–gel approaches at 500 °C [31–33]. However, the estimated value of the bandgap for the as-grown TiO_2 thin film is larger than bulk TiO_2 (3.3 eV), since the films consisting of fine crystallites show "blue shift" [34]. We assume that the increase in the bandgap is due to the quantum size effect (QSE), which occurs for semiconductor particles below 100 nm. No significant variance was observed between the optical bandgaps of the bare TiO_2 and WO_3 (0.1 M)/TiO_2 or TiO_2/WO_3 (0.1 M) bilayered films, which is expected due to the low crystallinity of WO_3. In particular, it has been reported that WO_3 has an energy bandgap that can fluctuate from 2.5 to 3.4 eV with variations in crystallinity, as amorphous WO_3 (3.2–3.4 eV) shows larger band-gap energy values than polycrystalline WO_3 (2.5–2.8 eV) [14, 35]. Moreover, the band-gap widening of WO_3 has previously been observed in the case of amorphous-like WO_3 in hybrid WO_3/TiO_2 samples for low loadings of WO_3 and this phenomenon was ascribed to structural fluctuation or high dispersibility of WO_3 particles on the TiO_2 surface [36]. However, in the case of the TiO_2/WO_3 (0.2 M) bilayers, standing for a higher loading of WO_3 compared to the TiO_2/WO_3 (0.1 M) ones, a shift to higher wavelengths was observed, which corresponds to a small decrease in the band-gap energy values and thus a higher absorbance of visible-light.

FE-SEM images of the films are presented in Fig. 4. TiO_2 deposited by a sol–gel route, as shown in Fig. 4a, led to a dense and homogeneous film with cracks, which can be attributed to the removal of residual hydroxyl and organic groups during the heat treatment process, while when WO_3 underlaid TiO_2 (WO_3/TiO_2), no morphological differences in comparison with the bare TiO_2 film were observed (see Fig. 4b). Moreover, WO_3, when deposited as an overlayer on TiO_2 from a 0.1 M precursor solution (TiO_2/WO_3), was present at the form of spherical structures on the TiO_2 surface. WO_3 particles showed a higher degree of aggregation from one (Fig. 4c) to two annealing steps (Fig. 4d), since the calcination at high temperature accelerates mass transfer and enhances the crystallization of tungsten oxides [14]. Finally, as the concentration of the tungsten trioxide precursor solution increased up to 0.2 M, the coverage of WO_3 particles on TiO_2 films appeared to proliferate, as presented in Fig. 4e.

We evaluated the photocatalytic activity of the TiO_2/WO_3 bilayered films under UV–Vis light by assessing the decolorization of methylene blue dye in aqueous solution. The photolytic removal of the dye in the absence of any photocatalyst was negligible, underlining the indispensability of the catalyst. Moreover, to eliminate the possibility of dye removal by adsorption on the catalyst surface, the films were placed at the bottom of the reactor under dark conditions and in contact with the dye for 40 min, during which time equilibrium of adsorption–desorption was reached. In all cases, removal was insignificant (less than 5%), pointing to the fact that the decolorization of the dye should be attributed to a pure photocatalytic regime.

As shown in Fig. 5a, when compared with a pure TiO_2 film, the layered TiO_2/WO_3 films were highly effective regarding the decolorization of MB. In addition, two annealing steps led to increased photoactivity of the films compared to one annealing step that can be attributed to their higher trend towards ordering, as pointed out by Raman spectroscopy. What is more, the effect of the position of the tungsten oxide layer on the photocatalytic performance of the bilayered films was assessed and the results are shown in Fig. 5b. When the WO_3 layer underlaid TiO_2, MB removal was lower (~66% decolorization after 300 min of irradiation), than in the case of an overlying WO_3 layer (~76%). These results verify that our bilayered system is effective in the removal of MB, contrary to the previous results for TiO_2 films overlaid by WO_3, for which no enhancement of the photocatalytic oxidation activities was reported compared to bare TiO_2 films [14]. Moreover, as presented in Fig. 6, upon increase of the concentration of the tungsten precursor solution to a threshold value of 0.1 M, an enhancement in the photocatalytic activity of the bilayered catalyst occurred (~76% conversion of the dye after 300 min of irradiation, versus ~59% in the case of a bare TiO_2 film). Above this threshold value, the photocatalytic efficiency of the composite films decreases, in good agreement with the literature [10, 37, 38].

A plausible explanation accounting for the observed better photocatalytic performance of the bilayered TiO_2/WO_3 films compared to bare TiO_2 can be attributed to a more efficient charge separation of photogenerated species. As previously mentioned, one of the most important factors that limit the photoactivity of TiO_2 is its high recombination rate of photoinduced charge carriers. When a semiconductor material is irradiated with a light source of an appropriate wavelength, excitation occurs and electrons (e^-_{cb}) migrate from the valence band to the conduction band of the material, leaving behind positively charged holes (h^+_{vb}). The photogenerated holes will thereafter react with OH^- or H_2O adsorbed on the surface of the catalyst, producing hydroxyl radicals that are mainly responsible for the degradation of the target pollutant. It is, therefore, expected that a high recombination rate of photogenerated holes and electrons will be detrimental for the performance of the photocatalyst.

Nevertheless, an efficient electron and hole transfer between WO_3 and TiO_2 depends on the difference between the conduction and valence band potentials of the two

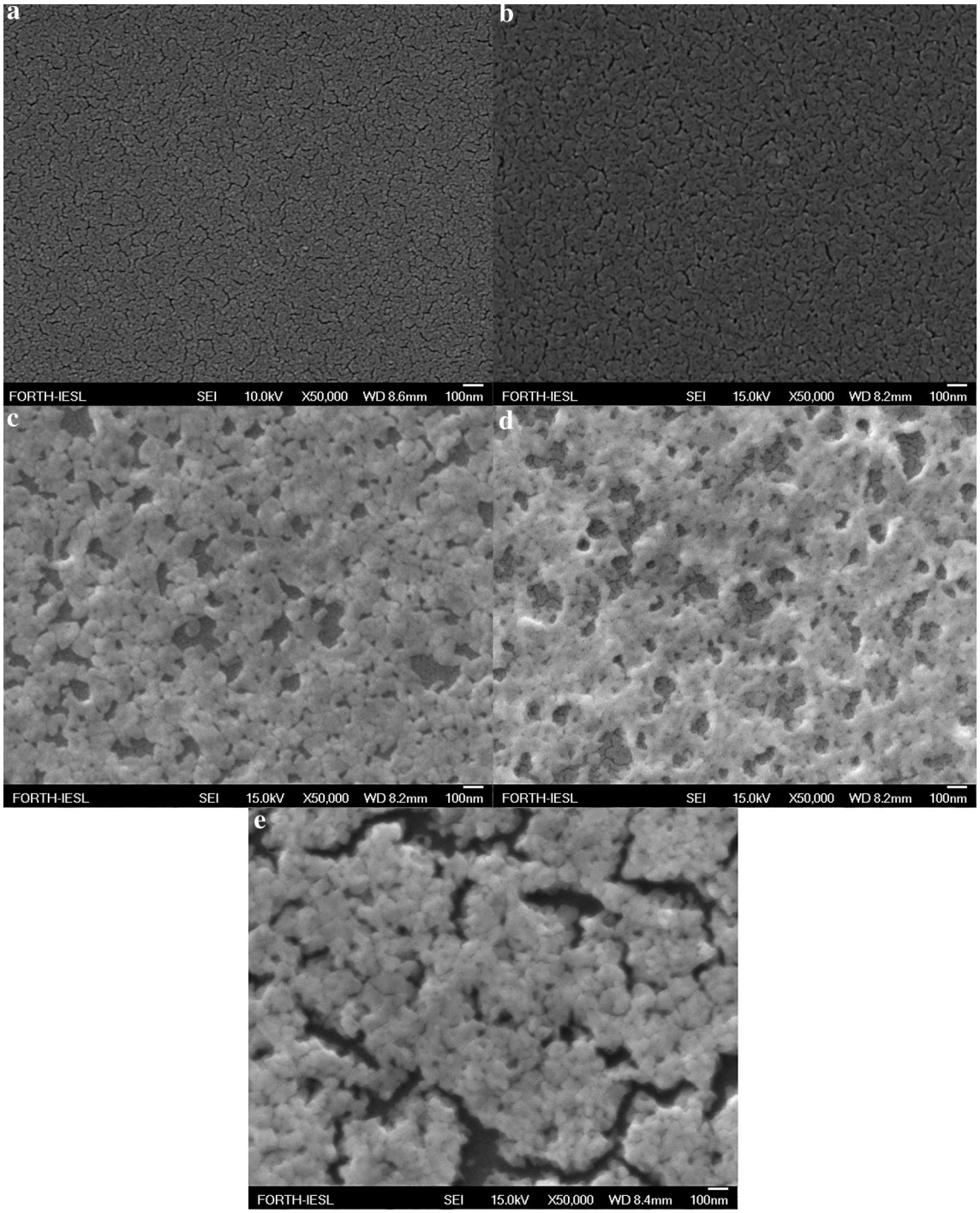

Fig. 4 SEM images of **a** bare TiO_2 film, **b** WO_3 (0.1 M)/TiO_2 bilayered film by two annealing steps and TiO_2/WO_3 (0.1 M) bilayered film by **c** one annealing step and **d** two annealing steps and **e** TiO_2/WO_3 (0.2 M) bilayered film by two annealing steps

semiconductors, respectively, that should be suitably positioned [39]. The valence band potential of WO_3 is more positive than that of TiO_2 and the conduction band of TiO_2 is more negative than that of WO_3, thus allowing charge separation and increasing the efficiency of the photocatalytic reaction [40]. Towards this direction, the coupling of TiO_2 and WO_3 can lead to a simultaneous electron transfer between the semiconductors with WO_3 acting as an electron trap, resulting, therefore, in an efficient separation of photogenerated charge carrier pairs, as presented in Fig. 7 [3]. In particular, the beneficial effect of WO_3 on the photocatalytic activity of a coupled WO_3–TiO_2 catalyst can

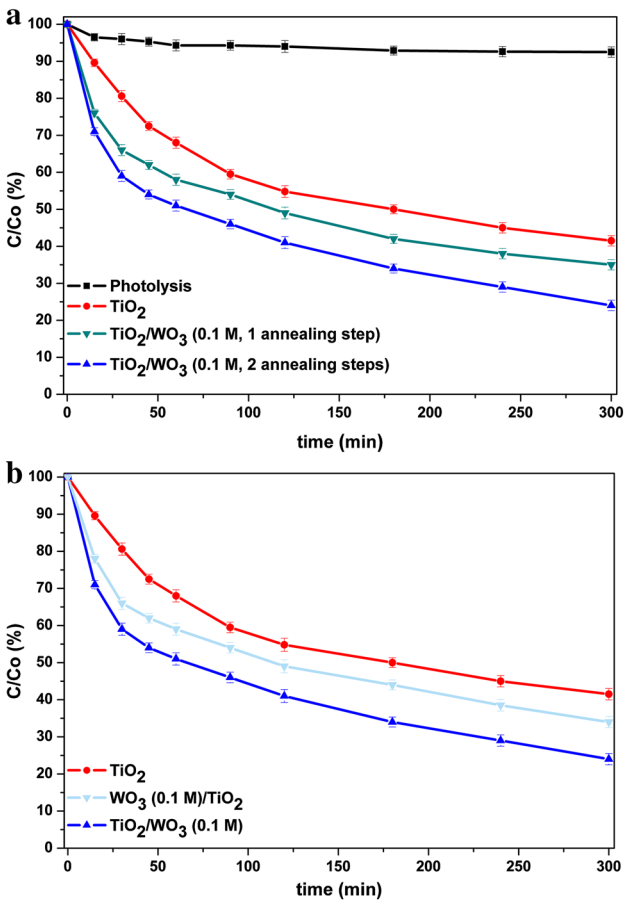

Fig. 5 Photocatalytic decolorization of methylene blue by **a** TiO_2/WO_3 (0.1 M) film by one and two annealing steps and **b** TiO_2/WO_3 (0.1 M) and WO_3 (0.1 M)/TiO_2 bilayers by two annealing steps. The photocatalytic results for the bare TiO_2 film and without a catalyst (photolysis) are also presented

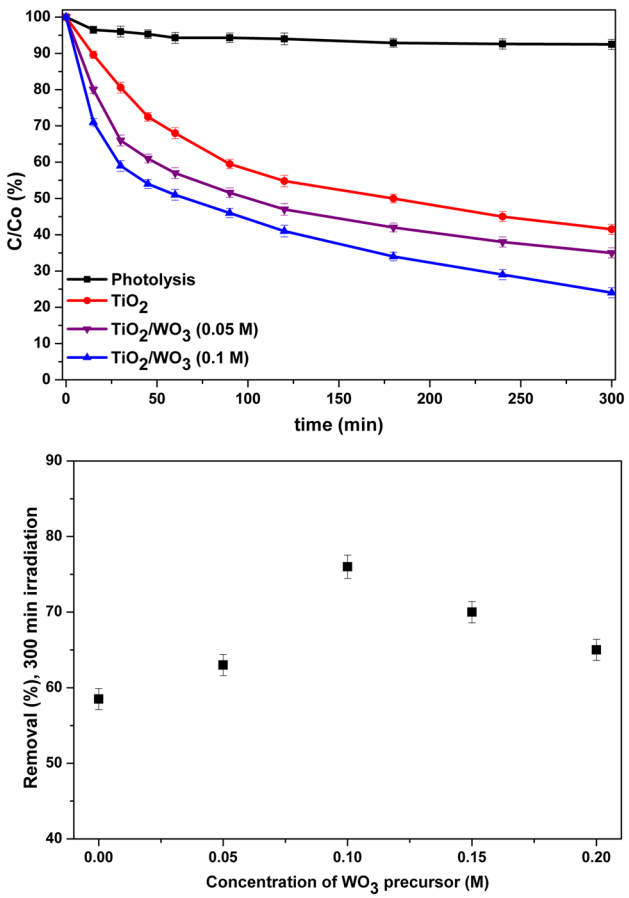

Fig. 6 Photocatalytic performance of TiO_2 and bilayered TiO_2/WO_3 films (overlying tungsten oxide layer, two annealing steps) for different tungsten precursor concentrations

be ascribed to its electron-accepting efficiency, since W^{6+} can be easily reduced in W^{5+}, as the standard reduction potential of W^{6+} to W^{5+} is only −0.03 V [41, 42]. These accumulated electrons at the conduction band of WO_3 can be consequently transferred to O_2 adsorbed on the surface, generating ·OH radicals. Moreover, the h^+ that are produced in the valence band of WO_3 can be transferred to the valence band of TiO_2 creating more ·OH radicals and thus enhancing the overall performance of the bilayered film [43, 44].

In our bilayered system, when the WO_3 layer underlaid TiO_2, the photocatalytic performance was lower than in the case of an overlying WO_3 layer. As was mentioned previously, TiO_2 formed relatively compact layers, while WO_3 aggregated in the form of islands. Therefore, with WO_3 as the outer layer, both oxides were well exposed to the dye solution and irradiation. In such surfaces, both oxidation and reduction reactions can easily proceed, as both the photogenerated electrons and holes could reach

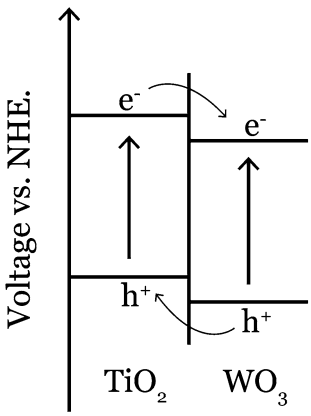

Fig. 7 Energy diagrams for TiO_2/WO_3 bilayered films

more easily the surface of the film to produce hydroxyl radicals and the photocatalytic oxidation reactions on the surface of the catalyst would be enhanced. In the same context, for the bilayered film with an underlying WO_3 layer where only TiO_2 is exposed, the reactions

associated with electrons on the surface of the film would be retarded, since the photogenerated e^- that were accumulated in the conduction band of WO_3 could be transferred less eagerly to the surface [45]. In accordance, a prolonged annealing of TiO_2/WO_3 films resulted in a higher degree of WO_3 aggregation and therefore better exposure of the TiO_2 surface, enhancing further the oxidation and reduction reactions. Finally, above an optimum WO_3 content, i.e., higher than the tungsten precursor concentration threshold value of 0.1 M, the photocatalytic performance of the bilayered films decreases, a phenomenon which is in agreement with the previous reports [38, 46]. This phenomenon can be attributed to a plausible screening effect because of the excess coverage of WO_3 on the TiO_2 layer, a claim that is also supported by the SEM image of the corresponding sample (Fig. 4e). Moreover, as mentioned above, in the bilayered TiO_2/WO_3 systems, WO_3 acts as an electron trap, promoting the effective separation of photogenerated electron–hole pairs and inhibiting their recombination. However, similar to a noble metal/titania composite system [47], higher tungsten oxide contents act as electron–hole recombination centers rather than facilitating charge transport, thus reducing the photocatalytic efficiency of the bilayered films.

Photoluminescence (PL) emission results from the recombination of photogenerated electrons and holes, and therefore, the PL emission spectra of our bilayered films were recorded to investigate the efficiency of charge carrier trapping, migration, and transfer [48]. The corresponding spectra are presented in Fig. 8, where a decrease of the PL intensity is observed for the bilayered films compared to the bare TiO_2 film. This is an indication of a reduced recombination rate of electrons and holes for the hybrid films, while the reduction of the PL intensity for each film is in good accordance with its quantified photocatalytic efficiency.

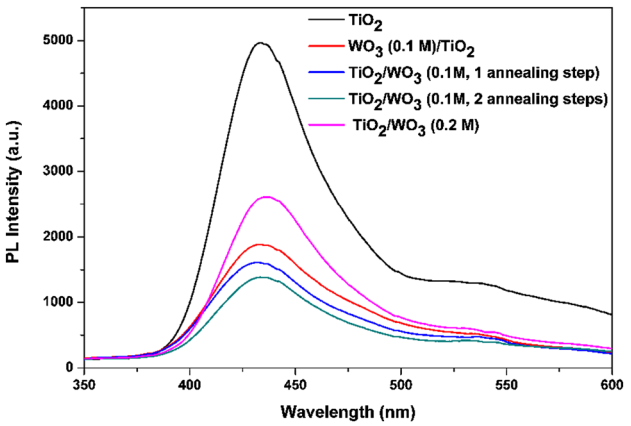

Fig. 8 Photoluminescence spectra of bare TiO_2 and bilayered TiO_2/WO_3 and WO_3/TiO_2 films

4 Conclusions

TiO_2/WO_3 bilayered films, composed of dense and homogeneous layers of anatase TiO_2 and monoclinic WO_3 in the form of spherical structures, were synthesized by a sol–gel method and deposited by spin-coating on Corning glass substrates. The photocatalytic efficiency of the bilayered films was evaluated by the removal of methylene blue dye under UV–Vis light irradiation. The implementation of two annealing steps for the bilayered films led to a higher degree of WO_3 aggregation and a higher exposure degree of both oxides to the dye molecules and the incident light irradiation compared to one annealing step, resulting, therefore, in better photoactivity. In addition, TiO_2 films with an overlying WO_3 layer demonstrated better photocatalytic performance than in the case of an underlying tungsten trioxide layer where only TiO_2 is exposed, as in such surfaces, both oxidation and reduction reactions can easily proceed due to the simultaneous exposure of both oxide layers. Furthermore, the decolorization rate increases with the WO_3 precursor solution concentration up to 0.1 M, but drops above this threshold value, as higher WO_3 contents may act as electron–hole recombination centers, thus reducing the photocatalytic efficiency of the bilayered system. In general, the hybrid TiO_2/WO_3 bilayered films deposited in this study showed enhanced photocatalytic efficiency compared to bare TiO_2 films. This can be attributed mainly to a more efficient electron and hole transfer mechanism, with WO_3 acting as an electron trap, facilitating charge transport and limiting charge recombination.

Acknowledgements This project is implemented through the Operational Program "Education and Lifelong Learning", Action Archimedes III and is co-financed by the European Union (European Social Fund) and Greek national funds (National Strategic Reference Framework 2007–2013). Ms. Aleka Manousaki and Ms. Maria Androulidaki are also gratefully acknowledged for assistance with SEM and PL measurements, respectively.

References

1. X. Chen, S.S. Mao, Chem. Rev **107**, 2891 (2007)
2. H.G. Oliveira, B.C. Fitzmorris, C. Longo, J.Z. Zhang, Sci. Adv. Mater **4**, 673 (2012)
3. S. Rawal, S. Bera, W. Lee, Catal. Lett **142**, 1482 (2012)
4. O. Mashtalir, M. Kurtoglu, S. Pogulay, A. Gogotsi, M. Naguib, Y. Gogotsi, Int. J. Appl. Ceram. Tech **10**, 26 (2013)
5. H. Yang, R. Shi, K. Zhang, Y. Hu, A. Tang, X. Li, J. Alloys Compd. **398**, 200 (2005)
6. I. Paramasivam, Y.-C. Nah, C. Das, N.K. Shrestha, P. Schmuki, Chem. Eur. J **16**, 8993 (2010)

7. S. Anandan, T. Sivasankar, T. Lana-Villarreal, Ultrason. Sonochem. **21**, 1964 (2014)
8. X. Luo, F. Deng, L. Min, S. Luo, B. Guo, G. Zeng, C. Au, Environ. Sci. Technol. **47**, 7404 (2013)
9. J. Cai, X. Wu, S. Li, F. Zheng, ACS Sustainable Chem. Eng **4**, 1581 (2016)
10. J.H. Pan, W.I. Lee, Chem. Mater **18**, 847 (2006)
11. L. Fu, W. Cai, A.W. Wang, Y.H. Zheng, L. He, Z.X. Fu, Mater. Technol. **30**, 264 (2015).
12. A.O.T. Patrocinio, L.F. Paula, R.M. Paniago, J. Freitag, D.W. Bahnemann, ACS Appl. Mater. Interfaces **6**, 16859 (2014)
13. A. Bojinova, C. Dushkin, React. Kinet. Mech. Catal. **103**, 239 (2011).
14. M. Miyauchi, A. Nakajima, K. Hashimoto, T. Watanabe, Adv. Mater **12**, 1923 (2000)
15. D. Vernardou, K. Vlachou, E. Spanakis, E. Stratakis, N. Katsarakis, E. Kymakis, E. Koudoumas, Catal. Today **144**, 172 (2009)
16. E.O. Zayim, Sol. Energy Mat. Sol. Cells **87**, 695 (2005).
17. A. Houas, H. Lachheb, M. Ksibi, E. Elaloui, C. Guillard, J.-M. Herrmann, Appl. Catal. B **31**, 145 (2001)
18. P. Kajitvichyanukul, J. Ananpattarachai, S. Pongpom, Sci. Technol. Adv. Mater **6**, 352 (2005)
19. L. Sun, T. An, S. Wan, G. Li, N. Bao, X. Hu, J. Fu, G. Sheng, Purif. Technol. **68**, 83 (2009).
20. A. Rampaul, I.P. Parkin, S.A. O'Neill, J. DeSouza, A. Mills, N. Elliott, Polyhedron **22**, 35 (2003)
21. B. Pecquenard, H. Lecacheux, J. Livage, C. Julien, J. Solid State Chem **135**, 159 (1998)
22. G. Schwarzenbach, J. Muehlebach, K. Mueller, Inorg. Chem **9**, 2381 (1970)
23. G. Kenanakis, N. Katsarakis, J. Env, Chem. Eng **2**, 1748 (2014)
24. D. Vernardou, G. Kalogerakis, E. Stratakis, G. Kenanakis, E. Koudoumas, N. Katsarakis, Solid State Sci. **11**, 1499 (2009).
25. H. Habazaki, Y. Hayashi, H. Konno, Electrochim. Acta **47**, 4181 (2002)
26. Y. Liu, C. Xie, H. Li, H. Chen, Y. Liao, D. Zeng, Appl. Catal. B **102**, 157 (2011)
27. M. Ocaña, J.V. Garcia-Ramos, C.J. Serna, J. Am. Ceram. Soc. **75**, 2010 (1992)
28. J. Zhang, M. Li, Z. Feng, J. Chen, C. Li, J. Phys. Chem. B **110**, 927 (2005)
29. D. Vernardou, E. Spanakis, G. Kenanakis, E. Koudoumas, N. Katsarakis, Mater. Chem. Phys **124**, 319 (2010)
30. D. Vernardou, H. Drosos, E. Spanakis, E. Koudoumas, C. Savvakis, N. Katsarakis, J. Mater. Chem **21**, 513 (2011)
31. G. Kenanakis, D. Vernardou, A. Dalamagkas, N. Katsarakis, Catal. Today Part A **240**, 146 (2015)
32. T. Giannakopoulou, N. Todorova, T. Vaimakis, S. Ladas, C. Trapalis, J. Sol. Energy Eng. **130**, 041007 (2008)
33. B.-H. Kim, J.-H. Ahn, J.-H. Jeong, Y.-S. Jeon, K.-O. Jeon, K.-S. Hwang, Ceram. Int. **32**, 223 (2006)
34. T. Wang, H. Wang, P. Xu, X. Zhao, Y. Liu, S. Chao, Thin Solid Films **334**, 103 (1998)
35. I. Shiyanovskaya, M. Hepel, J Electrochem. Soc. **146**, 243 (1999)
36. S. Higashimoto, Y. Ushiroda, M. Azuma, Top. Catal. **47**, 148 (2008).
37. F. Riboni, L.G. Bettini, D.W. Bahnemann, E. Selli, Catal. Today **209**, 28 (2013)
38. B. Grbić, N. Radić, S. Stojadinović, R. Vasilić, Z. Dohčević-Mitrović, Z. Šaponjić, P. Stefanov, Surf. Coat. Technol **258**, 763 (2014)
39. S. Rehman, R. Ullah, A.M. Butt, N.D. Gohar, J. Hazard. Mater. **170**, 560 (2009)
40. A.L. Linsebigler, G. Lu, J.T. Yates, Chem. Rev **95**, 735 (1995)
41. K. Tennakone, O.A. Ileperuma, J.M.S. Bandara, W.C.B. Kiridena, Semicond. Sci. Technol **7**, 423 (1992)
42. V. Keller, P. Bernhardt, F. Garin, J. Catal **215**, 129 (2003)
43. S. Anandan, M. Miyauchi, Chem. Commun **48**, 4323 (2012)
44. D. Tsukamoto, M. Ikeda, Y. Shiraishi, T. Hara, N. Ichikuni, S. Tanaka, T. Hirai, Chem. Eur. J. **17**, 9816 (2011).
45. M. Miyauchi, A. Nakajima, T. Watanabe, K. Hashimoto, Chem. Mater **14**, 4714 (2002)
46. S.A.K. Leghari, S. Sajjad, F. Chen, J. Zhang, Chem. Eng. J **166**, 906 (2011)
47. E. Vasilaki, I. Georgaki, D. Vernardou, M. Vamvakaki, N. Katsarakis, Appl. Surf. Sci **353**, 865 (2015)
48. F. Wang, X. Chen, X. Hu, K.S. Wong, J.C. Yu, Sep. Purif. Technol **91**, 67 (2012)